Dynamics of Energy Condensation in Two-Dimensional Turbulence

M. Chertkov,[1] C. Connaughton,[1] I. Kolokolov,[2,1] and V. Lebedev[2,1]

[1]*Theoretical Division & Center for Nonlinear Studies, LANL, Los Alamos, New Mexico 87545, USA*
[2]*Landau Institute for Theoretical Physics, Moscow, Kosygina 2, 119334, Russia*

(Received 9 January 2007; published 21 August 2007)

We report a numerical study, supplemented by phenomenological explanations, of "energy condensation" in forced 2D turbulence in a biperiodic box. Condensation is a finite size effect which occurs after the standard inverse cascade reaches the size of the system. It leads to the emergence of a coherent vortex dipole. We show that the time growth of the dipole is self-similar, and it contains most of the injected energy, thus resulting in an energy spectrum which is markedly steeper than the standard $k^{-5/3}$ one. Once the coherent component is subtracted, however, the remaining fluctuations have a spectrum close to k^{-1}. The fluctuations decay slowly as the coherent part grows.

DOI: 10.1103/PhysRevLett.99.084501 PACS numbers: 47.27.E−, 92.60.hk

A big difference between 2D and 3D turbulence is the generation of large scale structures from small-scale motions [1,2]. This occurs because, if pumped at intermediate scales, the 2D Navier-Stokes equations favor energy transfer to larger scales [3–6], a phenomenon known as an inverse cascade. Simulations [7,8] and experiments [9–11] show that large scale accumulation of energy is observed if conditions permit the energy to reach the system size. In this Letter, we study the "condensate" emerging in the form of two coherent vortices in a biperiodic box in 2D. Let us begin by briefly reviewing the classical 2D turbulence theory of Kraichnan, Leith, and Batchelor (KLB) [3–5]. The essential difference with 3D turbulence is the presence of a second inviscid invariant, in addition to energy, the enstrophy. Stirring the 2D flow leads to emergence of two cascades. Enstrophy cascades from the forcing scale, l, to smaller scales (direct cascade) while energy cascades from the forcing scale to larger scales (inverse cascade). Viscosity dissipates enstrophy at the Kolmogorov scale, η, which is much smaller than l when the Reynolds number is large. The energy cascade is blocked at a scale ζ, $\zeta \gg l$ by a frictional dissipation (usually due to friction between the fluid and substrate although other mechanisms can be imagined) after a transient in time quasistationary regime. Then a stationary KLB turbulence is established [3–5]. Applying Kolmogorov phenomenology (see, e.g., [1]) KLB predicts an energy spectrum scaling as k^{-3} in the direct cascade and as $k^{-5/3}$ in the inverse cascade. Here k is the modulus of the wave vector. The KLB spectra imply that velocity fluctuations at a scale r, δv_r scale as $\epsilon^{1/3} l^{-2/3} r$ and $(\epsilon r)^{1/3}$ in the direct and inverse cascade ranges, respectively. KLB theory is confirmed by simulations [12,13] and experiments [2,14], provided sufficient ranges of scales are available. If the frictional dissipation is weak so that ζ exceeds the system size L then ultimately the condensate regime emerges [3,7] where the standard KLB does not apply. Condensation in the 2D nonlinear Schrodinger equation was studied from the perspective turbulent cascades in [15].

A traditional motivation for studying 2D turbulence is its structural and phenomenological similarity to quasigeostrophic turbulence [16,17] in planetary atmospheres [18]. Recent interest specifically in the condensate state, however, was sparked by experimental [11] and numerical [19] observations of large scale coherent vortices associated with energy condensation in forced, bounded flows. In [11] the point is made that 2D spectral condensation is connected to the L-H (confinement) transition in magnetically confined plasmas which is often described by quasi-2D dynamics. In this Letter, we report a set of numerical experiments designed to give a clean, detailed study of energy condensation in its own right.

We solved the incompressible forced Navier-Stokes equations with hyperviscous dissipation in 2D:

$$\partial_t \boldsymbol{u} + (\boldsymbol{u} \cdot \nabla)\boldsymbol{u} + \boldsymbol{\nabla} p = \nu \Delta^8 \boldsymbol{u} + \boldsymbol{f} \qquad \boldsymbol{\nabla} \cdot \boldsymbol{u} = 0. \quad (1)$$

The domain is a doubly periodic box of size $L = 2\pi$. The forcing, $\boldsymbol{f}$, injects velocity fluctuations and energy at an intermediate scale l with energy injection rate ϵ. For the simulations shown in Figs. 1 and 3, $l = 2\pi/50$ and $\epsilon = 0.004$. We use a standard pseudospectral solver with full dealiasing. The resolution varied from 256^2 to 1024^2. For developed condensate computations, the resolution was only 256^2 owing to the requirement of integration for tens of thousands of forcing times, which was done using a third order Runge-Kutta integrator with integrating factors. The time step was decreased as the condensate grows such that it satisfies $\Delta t < c_0 \Delta x / u_{\max}$, where Δx is the grid spacing, $u_{\max}$ is the maximum velocity, and c_0 is conservatively taken in the range 0.2–0.5. Energy injection was done in a spectral band using a stochastic additive force with fixed amplitude and random phase. The correlation time is the numerical time step. Small-scale dissipation was provided by Δ^8 hyperviscosity which is not expected to affect the large scale behavior. Large scale damping,

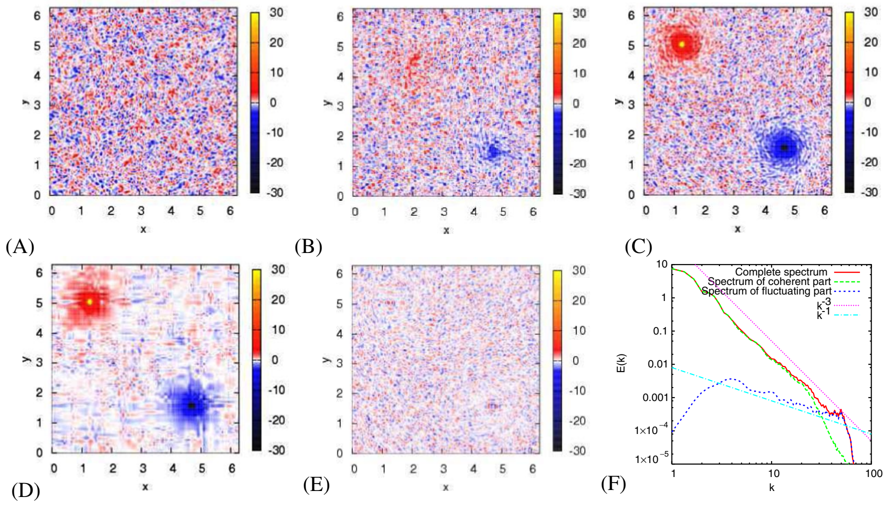

FIG. 1 (color online). Vorticity snapshots at a succession of times: (a) $t = 100$, (b) $t = 2000$, (c) $t = 10\,000$. Decomposition of the $t = 10\,000$ snapshot into coherent (d) and fluctuating parts (e). Energy spectra of the full field, coherent part and fluctuating part (f).

which is always present in physical experiments, does not prevent energy accumulation provided it is sufficiently weak [20]. The condensate grows without damping until it eventually saturates. Our investigations are relevant to this intermediate stage whereas the details of the damping are relevant to the final saturated stage.

The forcing is short correlated in time and characterized by the energy injection rate, ϵ, and the forcing scale, l. The majority of injected enstrophy cascades to smaller scales to be dissipated by viscosity. In our numerics, the closeness of η to l meant that only 40% of the injected energy goes upscale from l with the rest going downscale with the enstrophy. We simulate the zero friction case, assuring that the energy eventually piles up at the scale, L. The direct cascade sets up in a short time, $\tau_l \sim l^{2/3}/\epsilon^{1/3}$. The time, τ_*, for the inverse cascade to reach the scale, L, is much longer. Based on Kolmogorov arguments, $\tau_* \sim \epsilon^{-1/3}L^{2/3}$. In the simulations, $\tau_* \approx 1000$, in units where τ_l is about 1.

At $t > \tau_*$ we observed a condensate consisting of two big vortices having size of order L separated by a hyperbolic domain of comparable size. Figure 1(a), 1(b), and 2(c) illustrates the phenomenon with a series of vorticity snapshots. The condensate is formed to ensure that (a) the integral vorticity is zero in accordance with zero integral vorticity injected by the small-scale pumping and (b) the majority of energy brought by the inverse cascade is accumulated at the largest scale, L. Two identical vortices rotating in opposite directions satisfy these conditions. Because of biperiodicity, Fig. 1 actually depicts the emergence of a vortex crystal. Such crystals have been observed both numerically [8] and experimentally [10]. The vortices drift slowly over time but the square symmetry of the crystal is preserved by this drift.

Evolution of the vortices is slow relative to the background fluctuations which permits a separation of the flow into coherent and fluctuating components in the spirit of [21,22]. The highest amplitude coefficients of the wavelet transformed vorticity are assigned to the coherent component and the remainder to the incoherent component. Inverse wavelet transforms are then taken. This decomposition is shown in Fig. 1(d) and 1(e). Figure 1(e) shows that the fluctuating part is almost statistically homogeneous, whereas the coherent part is strongly inhomogeneous. This decompostion is insensitive, within reason, to the wavelet coefficient threshold owing to the strength of the vortices. Note that the characteristic amplitude of the vorticity fluctuations is larger than the coherent part of the vorticity over most of the domain. Ultimately we expect the coherent flow to dominate the fluctuations everywhere but we have not reached this regime.

As seen in Fig. 2(a), one observes $\propto \sqrt{t}$ growth of the maximum value of the coherent part of vorticity with time. Furthermore, simulations show the global growth $\propto \sqrt{t}$ of the coherent velocity profile. This global self-similarity is evident from Figs. 2(b) and 2(c). The law $\propto \sqrt{t}$ is naturally explained by the energy accumulation injected at the constant rate, ϵ, by forcing. In the hyperbolic region one estimates the coherent velocity as $\sqrt{\epsilon t}$.

The mean velocity profile within the vortex is almost perfectly circular. To a good precision higher order harmonics are suppressed relative to the zeroth order one. The velocity profile deduced from the simulations fits is $\propto r^{-\xi}$, where $\xi \approx 0.25$, in the range, $L \gg r \gg l$, and thus the vortex core is roughly l. This is illustrated in Fig. 2(d) showing the equivalent vorticity profile, $\propto r^{-1.25}$. We plot $r^{-1.25}$ profiles for two different forcing scales to check that the profile is insensitive to it.

So far, we have discussed the spatiotemporal features of the condensate. One may also analyze spectra. Time evolution of the spectrum is shown in Fig. 3(a), where one clearly sees transition at t_* from $k^{-5/3}$ to scaling steeper than $k^{-5/3}$ that is numerically close to k^{-3}. Similar statements were made before in Refs. [23,24]. This exponent

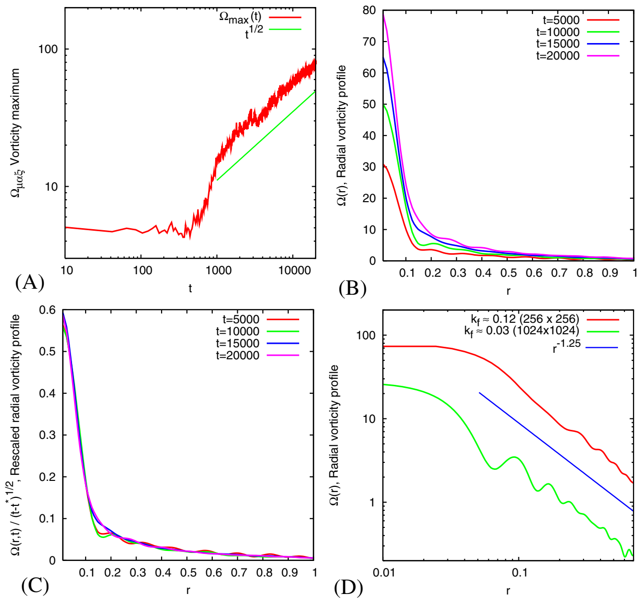

FIG. 2 (color online). Self-similar growth of the condensate. (a) Maximum vorticity as a function of time. (b) Angle-averaged vorticity, $\Omega(r)$, as a function of distance, r, from the vortex center for successive times. (c) Same profiles rescaled by $\sqrt{t - t^*}$. (d) $\Omega(r)$ in the developed condensate regime for 256×256 and 1024×1024 simulations with two different forcing scales.

does not signify a cascade in the KLB sense. From Fig. 3(b) we see that the energy flux to large scales remains constant with respect to k before and after t_*. The coherent part of the flow has almost no fluctuations and, if it is removed, the steeper than $k^{-5/3}$ scaling disappears entirely. By contrast, the k^{-3} enstrophy cascade of KLB involves fluctuating vortices across many scales.

The fluctuation spectrum is shown in Fig. 1(f); it is close to k^{-1}, a result obtained in [25] in decaying simulations. Fluctuations, while important for the energy flux, give a minor contribution to the overall energy, the majority of which is in the condensate as shown in Fig. 4(a). They contain more of the enstrophy as shown in Fig. 4(b), but they decay in amplitude as the condensate grows so that the flow becomes more and more coherent as time passes. The data suggest a logarithmic or weakly power law decay of the background fluctuations.

We now present an attempt to describe phenomenologically the universal nature of the asymptotic condensate state. Consider an individual vortex at $t \gg \tau_*$. It has a core of radius $\sim l$ and its spatial extent is estimated by the system size, L. In discussing the spatial structure of the vortex, for example, its mean vorticity profile, $\Omega = \langle \nabla \times \boldsymbol{u} \rangle$, we will track its dependence on the distance, r, from the center of the vortex, $\Omega(r)$. Once the almost circular vortex emerges, it sucks energy from the turbulent background which can be approximately described by an inhomogeneous eddy diffusivity, $D(r)$. Another large scale characteristic affected by the eddy diffusivity is the fluctuation enstrophy, $H(r) = \langle (\nabla \times \boldsymbol{u} - \Omega)^2 \rangle$. The focused regime is adiabatic so that the equations governing the quasistationary radially symmetric distribution of Ω and H on the top of the turbulent background are the eddy-diffusivity equations

$$\partial_r r D \partial_r \Omega = 0, \qquad \partial_r r D \partial_r H = 0. \tag{2}$$

D can be expressed in terms of the typical Lyapunov exponent, λ, $D \sim r^2 \lambda$. In homogeneous turbulence λ would be self-consistently estimated as $\sim\sqrt{H}$. However, the present situation is inhomogeneous, with a strong, $\sim\Omega$, shear. Mixing in the presence of strong shear was discussed in [26]. It was shown that the dependence of the effective Lyapunov exponent on the mean shear, $\sim\Omega$, and the background enstrophy, H, can be estimated as

$$\lambda \sim \begin{cases} H^{1/6}\Omega^{2/3}, & \tau_H \lambda \ll 1; \\ H^{1/4}\Omega^{1/2}, & \tau_H \lambda \gg 1. \end{cases} \tag{3}$$

Here τ_H is the correlation time of the background vorticity fluctuations. The actual nonparametric regime we are interested in is $\tau_H \lambda \sim 1$. Thus keeping the two asymptotics in Eq. (3) will, in fact, give upper and lower bounds. Returning to Eqs. (2) one notes that the physically meaningful solution of Eq. (2) for Ω corresponds to a flux state zero mode describing a constant flux of vorticity from the vortex center, $Dr\partial_r \Omega = \text{const}$ (with respect to r). On the

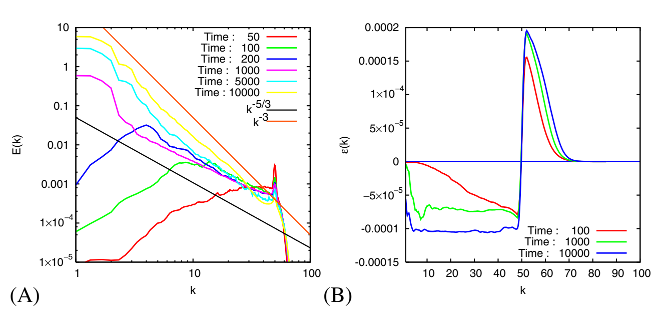

FIG. 3 (color online). (a) Evolution of the locally time averaged spectrum showing the transition from a $k^{-5/3}$ to a k^{-3} scaling at large scales. (b) Snapshots of the spectral energy flux.

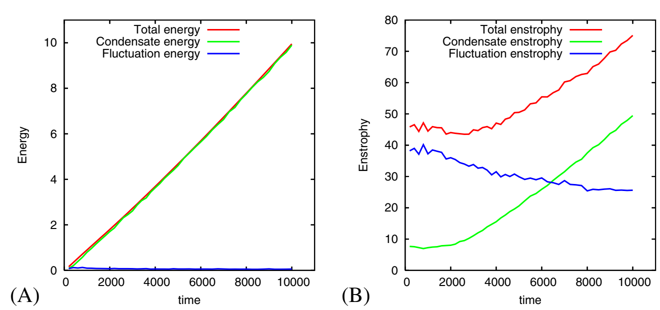

FIG. 4 (color online). (a) Time evolution of the energy contained in the condensate and background fluctuations (b) enstrophy.

contrary, the physically meaningful solution of the eddy-diffusivity equation for H is the one corresponding to a zero spatial flux, $H = \text{const}$ (with respect to r). Note that this spatially homogeneous distribution of H is in agreement with the results of simulations. Combining all these estimations with the global energy conservation one arrives at the following bounds

$$\Omega \sim \frac{\sqrt{\epsilon t}}{r}\begin{cases}(L/r)^{1/5}, & \tau_H\lambda \ll 1;\\ (L/r)^{1/3}, & \tau_H\lambda \gg 1.\end{cases} \quad (4)$$

These estimates for the mean vorticity profile are fully consistent, in describing both the overall temporal dynamics and the exponent of the mean vorticity profile, with the aforementioned numerical simulations, shown in Fig. 2: $1/5 < \xi \approx 0.25 < 1/3$. The corresponding estimate for the spatially homogeneous enstrophy, also expressing direct enstrophy balance at the pumping scale, is $H \sim \varepsilon/(l^2\lambda)$. This formula, combined with Eq. (3) for the Lyapunov exponent, predicts a slow algebraic decay of the background enstrophy in time. This is again consistent with simulations.

Finally, the spatial homogeneity of H suggests that majority of the injected enstrophy cascades to smaller scales, $r \ll l$. However, a subdominant portion will also penetrate to the larger scales, e.g., resulting in the k^{-1} spectrum observed in the simulations, see Fig. 3. An explanation of the k^{-1} spectrum observed at the scales larger than l after subtraction of the coherent component of the flow is as follows. In a range of scales smaller than L vorticity fluctuations are advected *passively*. Passive scalar theory, developed in [27], predicts an $\sim 1/r^2$ decay for the pair correlation of a scalar at the scales larger than injection scale in two dimensions and for nonzero value of the Corrsin invariant, which is the integral of the pair correlation function of the pumping. However, vorticity is a curl of velocity injection and thus the vorticity is injected at l with zero value of the Corrsin invariant. This leads to the localized, $\propto \delta(\boldsymbol{r})$, expression for the pair correlation function of vorticity, which in turn translates into the observed k^{-1} spectrum. The k^{-1} spectrum is the constant energy flux spectrum in the passive regime. Notice that a similar explanation for this scaling, referred to as passive inverse energy cascade, was reported in [28].

To conclude, we performed numerical simulations of energy condensation in forced 2D turbulence. We split the flow into coherent and fluctuating parts, observed the powerlike shape of the coherent vortices and self-similar growth in time of the coherent flow. As found in [23], these vortices are responsible for the k^{-3} spectrum observed in previous numerical experiments. The fluctuations have an energy spectrum of k^{-1} and they diminish in amplitude as the condensate grows. We also presented phenomenological description of the results.

We thank A. Celani, E. Lunasin, and L. Smith for advice on numerics and R. Ecke, G. Eyink, G. Falkovich, and M. Shats for helpful discussions. This work was carried out under the auspices of the National Nuclear Security Administration of the US Department of Energy at Los Alamos National Laboratory under Contract No. DE-AC52-06NA25396. I. K. and V. L. acknowledge partial support from RFBR Grant No. 06-02-17408-a.

[1] U. Frisch, *Turbulence: The Legacy of A. N. Kolmogorov* (Cambridge University Press, Cambridge, England, 1995).
[2] H. Kellay and W. I. Goldburg, Rep. Prog. Phys. **65**, 845 (2002).
[3] R. H. Kraichnan, Phys. Fluids **10**, 1417 (1967).
[4] C. E. Leith, Phys. Fluids **11**, 671 (1968).
[5] G. K. Batchelor, Phys. Fluids **12**, II-233 (1969).
[6] S. Chen, R. Ecke, G. Eyink, M. Rivera, M. Wan, and Z. Xiao, Phys. Rev. Lett. **96**, 084502 (2006).
[7] L. M. Smith and V. Yakhot, Phys. Rev. Lett. **71**, 352 (1993).
[8] L. M. Smith and V. Yakhot, J. Fluid Mech. **274**, 115 (1994).
[9] J. Paret and P. Tabeling, Phys. Fluids **10**, 3126 (1998).
[10] D. Z. Jin and D. H. E. Dubin, Phys. Rev. Lett. **84**, 1443 (2000).
[11] M. G. Shats, H. Xia, and H. Punzmann, Phys. Rev. E **71**, 046409 (2005).
[12] G. Boffetta, A. Celani, and M. Vergassola, Phys. Rev. E **61**, R29 (2000).
[13] G. Boffetta, arXiv:nlin/0612035v1.
[14] C. H. Bruneau and H. Kellay, Phys. Rev. E **71**, 046305 (2005).
[15] A. Dyachenko and G. Falkovich, Phys. Rev. E **54**, 5095 (1996).
[16] M. Lesieur, *Turbulence in Fluids* (Kluwer, Dordrecht, 1997).
[17] J. Charney, J. Atmos. Sci. **28**, 1087 (1971).
[18] G. Nastrom and K. Gage, J. Atmos. Sci. **42**, 950 (1985).
[19] D. Molenaar, H. J. H. Clercx, and G. J. F. van Heijst, Physica (Amsterdam) **196D**, 329 (2004).
[20] S. Danilov and D. Gurarie, Phys. Rev. E **63**, 061208 (2001).
[21] M. Farge and G. Rabreau, C.R. Acad. Sci. Ser. B **307**, 1479 (1988).
[22] M. Farge, K. Schneider, and K. Kevlahan, Phys. Fluids **11**, 2187 (1999).
[23] V. Borue, Phys. Rev. Lett. **72**, 1475 (1994).
[24] C. V. Tran and J. C. Bowman, Phys. Rev. E **69**, 036303 (2004).
[25] C. Beta, K. Schneider, and M. Farge, Communications in Nonlinear Science and Numerical Simulation **8**, 537 (2003).
[26] M. Chertkov, I. Kolokolov, V. Lebedev, and K. Turitsyn, J. Fluid Mech. **531**, 251 (2005).
[27] G. Balkovsky, E. Falkovich, V. Lebedev, and M. Lysiansky, Phys. Fluids **11**, 2269 (1999).
[28] S. Nazarenko and J.-P. Laval, J. Fluid Mech. **408**, 301 (2000).